Surface Plasmon Tunability of Core-Shell Au@Mo(6) Nanoparticles by Shell Thickness Modification

Flavien Sciortino, Ovidiu Cretu, Vasilios Karanikolas, Fabien Grasset, Stéphane Cordier, Katsuhiko Ariga, Takashi Kuroda, Koji Kimoto

Surface Plasmon Tunability of Core-Shell Au@Mo_6 Nanoparticles by Shell Thickness Modification

Flavien Sciortino[1,2], Ovidiu Cretu[3*], Vasilios Karanikolas[4*], Fabien Grasset[5,6], Stéphane Cordier[6], Katsuhiko Ariga[1,7], Takashi Kuroda[8], Koji Kimoto[3]*

1. International Center for Materials Nanoarchitectonics (WPI-MANA), National Institute for Materials Science (NIMS), Namiki 1-1, Tsukuba, Ibaraki 305-0044, Japan

2. Université Grenoble Alpes, CNRS, DCM UMR 5250, Grenoble F-38000, France

3. Research Center for Advanced Measurement and Characterization, National Institute for Materials Science (NIMS), Namiki 1-1, Tsukuba 305-0044, Japan

4. International Center for Young Scientists (ICYS), National Institute for Materials Science (NIMS), Namiki 1-1, Tsukuba 305-0044, Japan

5. CNRS - Saint-Gobain - NIMS, IRL 3629, Laboratory for Innovative Key Materials and Structures (LINK), National Institute for Materials Science (NIMS), 1-1 Namiki, Tsukuba, Ibaraki 305-0044, Japan

6. Univ. Rennes - CNRS - Institut des Sciences Chimiques de Rennes (ISCR), UMR 6226, Rennes F-35000, France

7. Department of Advanced Materials Science, Graduate School of Frontier Sciences, The University of Tokyo, 5-1-5 Kashiwanoha, Kashiwa, Chiba 277-8561, Japan

8. Research Center for Functional Materials, National Institute for Materials Science (NIMS), Namiki 1-1, Tsukuba 305-0044, Japan

AUTHOR INFORMATION

Corresponding Author

*flavien.sciortino@univ-grenoble-alpes.fr *Université Grenoble Alpes, CNRS, DCM UMR 5250, Grenoble F-38000, France

*cretu.ovidiu@nims.go.jp *Research Center for Advanced Measurement and Characterization, National Institute for Materials Science (NIMS), Namiki 1-1, Tsukuba 305-0044, Japan

*karanikolas.vasileios@nims.go.jp *International Center for Young Scientists (ICYS), National Institute for Materials Science (NIMS), Namiki 1-1, Tsukuba 305-0044, Japan

ABSTRACT

Plasmon resonances of noble metal nanoparticles are used to enhance the light-matter interactions in the nanoworld. The nanoparticles' optical response depends strongly on the dielectric permittivity of the surrounding medium. We show that the plasmon resonance energy of core-shell Au@Mo_6 nanoparticles can be tuned from 2.4 eV to 1.6 eV by varying the thickness of their Mo_6 cluster shells between zero and 70 nm, when the core diameter is fixed at 100 nm. We probe their plasmonic response by performing nanometer-resolution plasmon mapping on individual nanoparticles, using electron energy-loss spectroscopy inside a transmission electron microscope. Our experimental results are corroborated by numerical simulations performed using boundary element methods. The simulations predict a similar dependency for the extinction energy, showing that this effect could also be observed by light-

optical experiments outside the electron microscope, although limited by the size distribution of the nanoparticles in solution and the substantial scattering effects.

TOC GRAPHIC

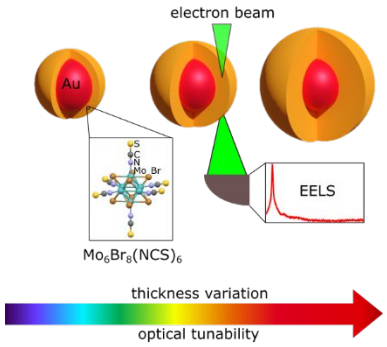

KEYWORDS core-shell nanoparticles, molybdenum octahedral clusters, surface plasmon, resonance tuning, electron energy-loss spectroscopy (EELS)

Noble metal nanoparticles have been (intentionally or accidentally) used for their optical properties since antiquity.[1] These properties were first explained in the early 1900s by Mie and can be understood on the basis of plasmon resonances.[2] The optical properties of noble metal nanoparticles are dominated by localized plasmon resonance (LPR) modes, hybrid modes of the electromagnetic field and the conduction band electrons of the metal. These modes are confined

at the interface between the metal and the dielectric host medium. A large body of work exists on this topic, along with many review articles[3,4] and books.[5] While most measurements are performed using light-optical techniques, electron microscopy has also provided interesting results,[6] due to the possibility of observing plasmons using electron energy-loss spectroscopy (EELS).[7] The first clear excitation of the plasmon polariton modes was achieved using a nearby placed electron beam.[8] An important advantage is the ability of an electron microscope to perform such measurements on single particles, while optical methods inevitably provide an average over a large volume, where the particle distribution leads to additional broadening of the optical signal. On an even lower scale, it is now routine to use such an instrument and map the distribution of the various plasmonic modes at the nanometer level.[9,10]

M_6 octahedral transition metal atom clusters display unique structural and physical properties which can vary with the nature of the metal as well as with the nature of the capping ligands.[11,12,13,14] This makes them interesting molecular building blocks for the functionalization of hybrid nanomaterials or for the structuring of functional surfaces at the nanoscale. $A_2Mo_6X_{14}$ ternary halides containing face-capped $[\{Mo_6X^i_{12}\}X^a_6]^{2-}$ cluster based units (A = alkali, X= Br, I, with "*i*" for face-capped inner ligands and "*a*" for apical ligands) are prepared by solid-state

synthesis.[15] The apical ligands X^a can be later modified in solution by functional organic or inorganic ligands L (e.g., L = X, CN, NCS, R-COO (R = C_nF_{2n+1}, polymerizable or mesogenic function))[16,17,18] in order to tune the physico-chemical properties, to favor their self-assembly,[19,20] their integration into inorganic matrices,[21] or to strengthen their interaction with semiconducting nanoparticles[22] or plasmonic surfaces.[23]

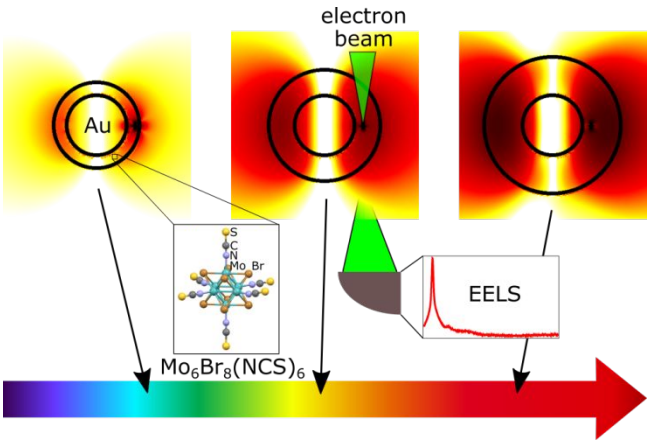

Figure 1. Schematic representation of the experimental methods and results. (upper half) Electromagnetic field distribution created by a focused electron beam (modeled as a dipole source) when interacting with nanoparticles of increasing shell thickness. (lower half) Representative values of the plasmon resonance wavelength (measured by EELS) for particles with increasing shell thickness studied in this work.

Au nanospheres can be used as building blocks for different applications, in sensing, light emitting and harvesting devices, etc. Their important features are the LPRs which are used to promote the light-matter interactions. For each application, the Au nanospheres need to have the LPR resonance at a specific energy, which depends on their geometrical characteristics and on the value of the dielectric permittivity of the host media. Increasing the value of the dielectric permittivity of the surrounding media leads to a redshift of the LPR energy.[4] However, functionalizing the Au spheres using their host medium severely limits their applications. Previous works have observed changes in optical properties characterized by shifts of the plasmon peak with the size[24,25] or aspect ratio[26] of the object, due to the length over which the resonance takes place, including recent results for the case of very small particles.[27] On the other hand, metallic bodies are expected to enhance the radiative emission of nearby placed localized photon sources. For Au spheres, which are used extensively as building blocks of nanodevices, the highest enhancement value has been predicted for a diameter of about 100 nm,[28] which provides incentives for keeping the size close to this value.

Au nanoparticles have been used extensively in core-shell studies, and there have been several previous reports on the effects of shell thickness on the plasmon resonance energy.[29-34] Large

tuning ranges of around 100 nm for the plasmonic resonance wavelength have been reported for Au@Ag,[29,30] as well as Au@Cu_2O nanoparticles.[31] All these studies concern measuring extinction/absorption spectra where the nanoparticles are in solution. The main difference with the present work is that we observe a much higher tuning range of around 250 nm in our experiments. One of the reasons is our single-particle TEM technique, which can be used to examine objects which are far from the average properties of the nanoparticles in solution; this aspect will be discussed in detail below.

In this study we show that a high level of tunability can be achieved for core-shell Au@Mo_6 particles with very similar core sizes, by varying the thickness of the shell, as summarized in Figure 1. We utilize the isothiocyanate terminated cluster-based building blocks $[Mo_6Br^i_8(NCS)^a_6]^{2-}$ in order to functionalize Au nanoparticles by creating a shell composed of Mo_6 clusters.[23] The $[Mo_6Br^i_8(NCS)^a_6]^{2-}$ anionic units are characterized by a $\{Mo_6Br^i_8\}^{4+}$ cluster core and each Mo atom is bonded to terminal NCS^- groups by Mo-C bonds. The pendant S atoms exhibit a high affinity to Au.[23] The optical response of the nanoparticles can also be excited by plane-wave far-field illumination, and a comparison is given between their response to a plane

wave and an electron beam excitation. Our results provide further proof for the versatility of these structures.

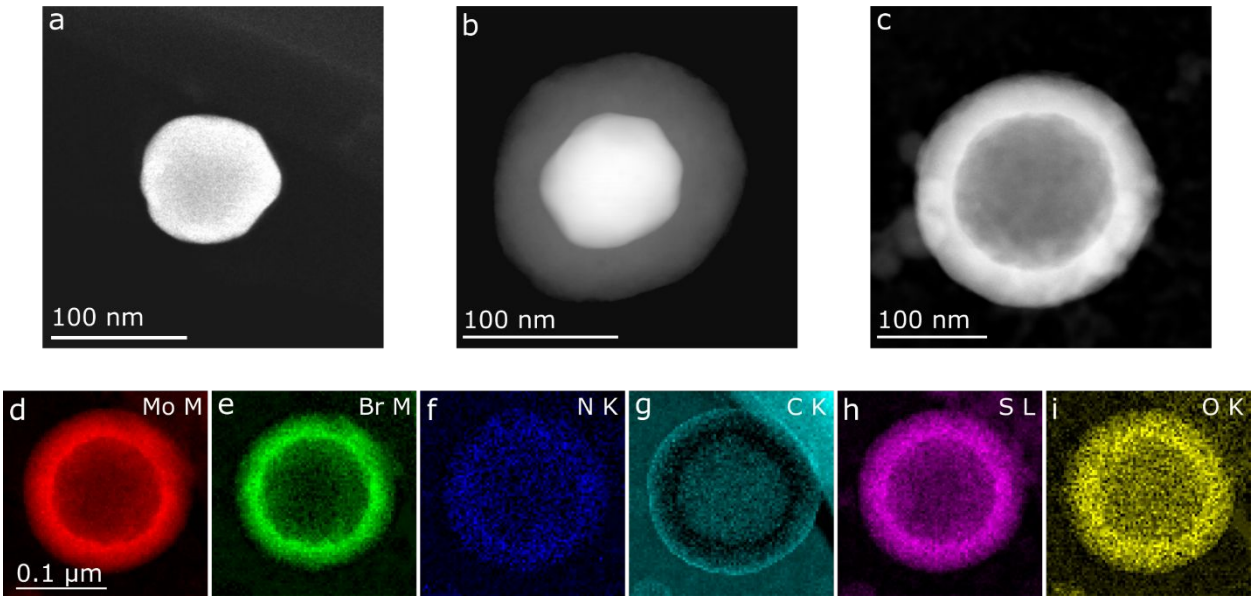

Figure 2. Representative HAADF images of bare Au nanoparticles (a), core-shell Au@Mo_6 nanoparticles (b) and empty shells (c). (d-i) Elemental maps of the area in (c), using core-loss EELS signals.

Representative images of the samples studied in this work are shown in Figure 2 and Figure S1. The main objects of interest are the bare (Figure 2a) and core-shell (Figure 2b) Au@Mo_6 nanoparticles. An important detail is that the (commercial) nanoparticle solution used has a very narrow diameter distribution, which we verified in Figure S3b. This avoids effects due to changes in particle size, which will be discussed in detail below.

As reported previously,[20] it is possible to also synthesize empty shells made of the same material as the nanoparticle coating (Figure 2c). This was used in order to check the chemical composition of the material. The relatively large number of elements present have overlapping peaks or edges in both EDS and EELS, which are the main elemental analysis techniques in a TEM. We have overcome this problem by using core-loss EELS and performing multiple linear least squares (MLLS) fitting, as shown in Figure S2. The results are shown in Figure 2d-i, confirming that all of the expected elements for this material are present and correctly distributed. An interesting observation can be made regarding oxygen, which is not expected in the formula. As reported previously,[20] the hydrolysis of $[Mo_6Br^i_8(NCS)^a_6]^{2-}$ is very slow but possible, leading to the substitution of some NCS by OH. Another possibility is that trace amounts of H_3O^+ could play the role of counter-cations in the shell.

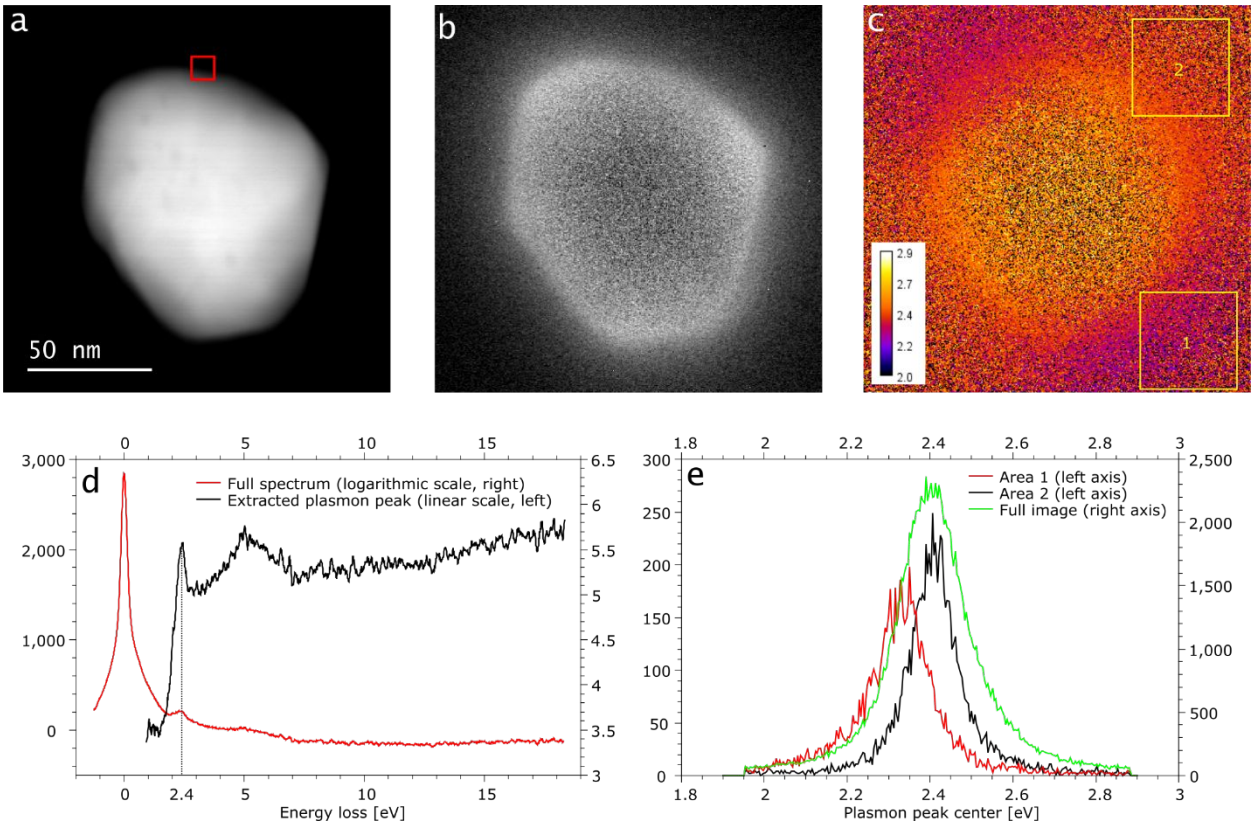

Figure 3. HAADF image (a), plasmon peak intensity (b) and plasmon peak position (c) for a bare Au nanoparticle. (d) EELS spectrum extracted from the area marked by a red square in (a). (e) Plasmon position histograms extracted from different areas in (c).

The plasmon mapping results for a bare Au nanoparticle are summarized in Figure 3. A HAADF image acquired at the same time as the EELS data is displayed in Figure 3a. As described in the Methods section, this particle is supported by a thin carbon film which is not visible in this image due to the strong contrast of the Au particle. A contrast-enhanced version of the same image does not show any carbon contamination surrounding the particle, in line with our efforts to avoid this

by heating the samples prior to observations. This is important since, at the nanometer scale, carbon contamination is very difficult to avoid in an electron microscope.[35] Furthermore, this phenomenon is proportional to the electron dose, which for a low-loss spectrum image is 10x-100x higher than for a standard image.

An EELS spectrum extracted from the area marked by a red square in Figure 3a is shown in Figure 3d. The full spectrum is displayed on a logarithmic scale in red, in order to accommodate the much higher signal of the ZLP. The spectrum obtained after subtracting the ZLP tail is displayed on a linear scale, in black. A sharp plasmon peak is immediately visible around 2.4 eV; an intensity map of this peak is shown in Figure 3b. By comparing to Figure 3a, we observe that this peak is concentrated around the surface of the particle, which is in line with both theory[4] and previous observations.[36]

Additional details can be obtained by mapping the energy of the plasmon peak, in Figure 3c. It is obvious that there are areas where the energy values are quite different, such as the ones marked "1" and "2" in this image. The differences could be explained by the different crystal facets which are close to these areas, in accordance with previous observations.[37] The histograms for these areas are plotted in Figure 3e, which additionally shows the histogram of the entire image,

from where the average plasmon energy for this nanoparticle can be measured to around 2.4 eV. These average energy values are the ones that we report throughout this study, in order to avoid any shape-related local effects. We have repeated the same procedure on several bare particles and found very similar values, despite their different shapes and orientations (Figure 5c).

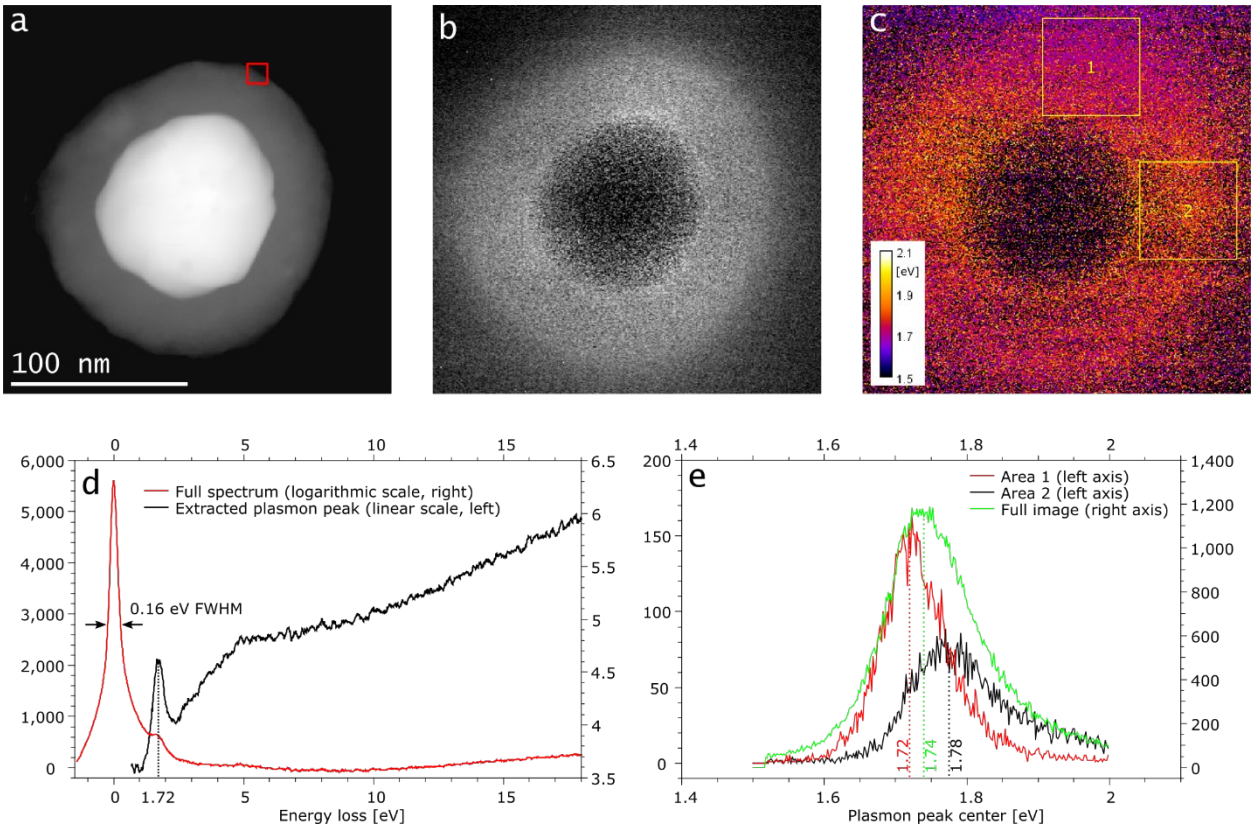

Figure 4. HAADF image (a), plasmon peak intensity (b) and plasmon peak position (c) for a core-shell Au@Mo_6 nanoparticle. (d) EELS spectrum extracted from the area marked by a red square in (a). (e) Plasmon position histograms extracted from different areas in (c).

The equivalent process of plasmon mapping in core-shell Au@Mo_6 particles is illustrated in Figure 4. The main difference between this and the previous case is the plasmon amplitude distribution in Figure 4b. Like in the case of bare particles, the signal is the highest close to the surface of the core, but it maintains significant amplitude in the area covered by the shell. This is better illustrated by the radially-averaged plots in Figure S4. Figure S4a shows the case of the bare nanoparticle in Figure 3; the normalized plasmon intensity (red curve) reaches a maximum slightly inside the surface of the particle and then decays in the vacuum. In Figure S4b, which shows the core-shell Au@Mo_6 particle in Figure 4, the same curve has a maximum just before the Au core limit, decays slowly inside the shell and then much rapidly in the vacuum. Two observations are in order. Firstly, it appears that the plasmon decay rate in vacuum is similar for the two cases, which is to be expected. Secondly, Figure S4b illustrates the importance of normalizing the EELS signal: the unprocessed plasmon amplitude (green curve) has a maximum close to the outer surface of the shell, which does not make physical sense and only occurs because of the strong scattering of the electron beam by the Au core away from the spectrometer entrance aperture.

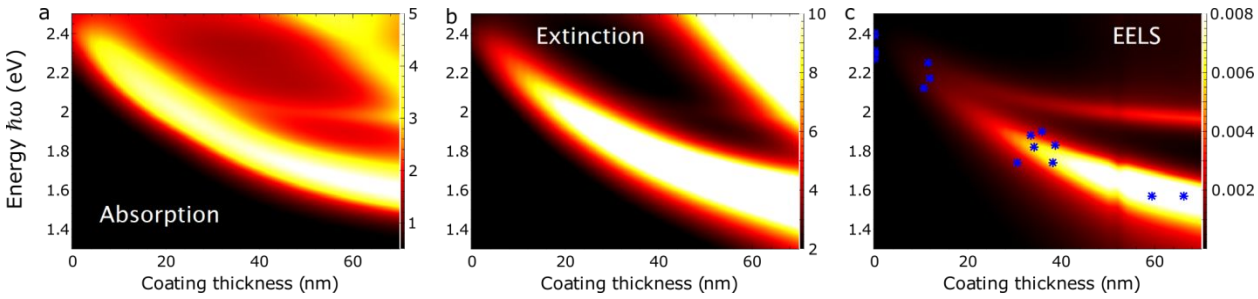

Figure 5. Contour plots of the absorption (a), extinction (b) and EELS spectra (c) calculations for a 100 nm Au nanoparticle surrounded by a shell of varying thicknesses, for different excitation energies. The experimentally measured EELS plasmon energy peak positions for the relevant coated thickness are overlaid as blue points in panel (c).

The main result of this work is shown in Figure 5. In Figure 5a, we present a contour plot of the numerically calculated absorption spectrum of the coated nanoparticle, in which the excitation energy and the coating thickness of the cluster material are varied. The Au-core cluster coated sphere supports surface plasmon modes, which appear as peaks in the absorption spectrum, shown in the contour plot by the brightest color. In Figure 5b we present a contour plot of the extinction of the Au core cluster coated sphere, where we again vary the excitation energy and the coating thickness. The extinction is defined as the sum of the absorption and scattering, and is the quantity typically measured using standard optical techniques, when nanoparticles are immersed in a solution. Here, we consider their optical response in air, in order to directly

compare with the EELS spectra. We observe that, due to the size of the sphere, the light-matter interaction is substantially influenced by the scattering processes that lead to a broadening of the LPR in the extinction spectra, for a given cluster thickness, compared to the absorption spectra of Figure 5a. Finally, in Figure 5c we present a contour plot of the numerically calculated EELS spectra,[7] considering an electron beam passing close to the Au core, penetrating 2 nm inside the cluster coating. We observe that the electron beam excites the LPR mode of the coated Au sphere through the high *k*-vector component of its near field and appears as a peak of its energy loss spectrum.

There is very good agreement between the measured and calculated EELS peak positions in Figure 5c. For a bare Au sphere placed in vacuum, the measured 2.4 eV (517 nm) plasmon energy agrees with earlier reports.[4,38] As the thickness of the cluster is increased, the plasmon peak converges to a constant measured value of 1.6 eV, matching the predicted resonance for a Au sphere immersed in a homogeneous dielectric medium with ε=5.5.[4] This effect allows us to confirm the dielectric permittivity of the cluster-based shell used in our numerical calculations.

The calculated extinction spectra of Figure 5b show a similar trend with Figure 5c, which proves that our observations are not limited to EELS measurements, and would be accessible by light-

optical experiments outside the TEM. Both EELS and absorption spectra can be used to accurately probe the surface plasmon mode. However, the absorption of the nanoparticles when immersed in a solution cannot be readily extracted because of the contribution of the scattering, which dominates for larger particles such as the ones studied here. There are, of course, fundamental differences between the two methods: extinction measurements probe the far-field response of the nanoparticle, while in EELS the electron passing at high speed through the sample is equivalent to a near-field excitation with deep-UV light.[7] The plasmon resonance energy of Au nanospheres can also be controlled by changing the dielectric permittivity value of the material they are immersed in,[4] or by covering them with films of different thicknesses.[39] Here, we show that the localized surface plasmon resonance energy of the Au sphere can be tuned over an energy rage of 0.8 eV by changing the coating material thickness, which provides a much more convenient alternative. It is important to mention that, due to the uniform Au core sizes, the localized plasmon resonance tunability is solely due to the shell thickness. In order to verify this, Figure S3a plots the plasmon energy for the same nanoparticles as a function of the core size, resulting in a random distribution.

A comparison between TEM measurements of the core-shell Au@Mo_6 plasmonic response and conventional measurements of their extinction spectra is given in Figure S5. We used SEM imaging in order to analyze a large number of particles and obtain a representative diameter distribution (Fig. S5a,b). The data shows that the average shell thickness is around 11 nm, which is much lower than some of the particles we analyzed by TEM. We also measured the optical absorption spectra of bare Au and core-shell Au@Mo_6 nanoparticles in solution (Fig. S5c). The absorption peak of the latter is broadened mainly due to the presence of many un-reacted Au particles, which fits with our SEM observations, where we found many Au particle clusters which did not have individual shells. After subtracting the bare particle peak, the remaining spectrum matches well with our simulations for Au@Mo_6 nanoparticles with a 11 nm thick shell (Fig. S5d). Comparing the values given by the two techniques for bare and core-shell particles with an 11 nm shell thickness, we find that in each of the two cases the EELS data shows plasmonic resonances at higher energies compared to the extinction spectra; this effect can be explained by the difference in the surrounding medium (vacuum vs. water), as well as by the different responses probed by the two techniques, i.e. near-field for EELS vs. far-field for the extinction spectra. Interestingly, the change in wavelength due to the presence of the shell is

almost identical between the extinction and EELS spectra for a shell thickness of 11nm. The different shell thicknesses of the nanoparticles only produce a broadening of the extinction spectra, while from the EELS spectra of single particles their effect in shifting the plasmonic resonance energy as function of the shell thickness is clearly observed. This information is lost when analyzing the extinction spectra of the core-shell structures. This shows that the ensemble measurements, while providing a more accurate average picture of the sample, show only a small part of the full range of the effects which can be seen from our single-particle TEM data.

Our observations for plasmon shifts in core-shell Au@Mo_6 particles can be understood analytically on the basis of the different dielectric functions of the core, shell, and medium.[40] The additional dielectric constant of the shell changes the condition required for plasmon resonance and introduces a dependency on the ratio of the shell volume to the total volume of the particle, as calculated in detail.[41,42] Considering a constant core radius, as in the case in the present experiments, this results in a dependency on the thickness of the shell, which is what we observe experimentally.

In summary, we have shown that we are able to tune the surface plasmon resonance of core-shell Au@Mo_6 nanoparticles over a large area of the visible spectrum by changing the thickness of the

shell. Moreover, this interval can be further shifted by utilizing Au nanoparticle cores of a different diameters, providing for an increased tuning range. Our observations add to the already impressive list of plasmonic properties of these structures. While mapping plasmons in the TEM is arguably more difficult than light optical experiments, it comes with the advantage of being able to probe the near-field response of single nanoparticles at the nanometer level. This opens the way for interesting systems consisting of particles with different sizes, different geometries, or different materials, which are coupled together, that can only be analyzed on a case-by-case basis due to their heterogeneity.

EXPERIMENTAL METHODS

Citrate-stabilized Au nanoparticles were purchased from Sigma-Aldrich and used as received. The starting cluster precursor $(NH_4)_2[Mo_6Br^i_8(NCS)^a_6]$ was prepared from the ternary bromide $Cs_2[Mo_6Br^i_8Br^a_6]$ by interaction with NH_4NCS in a H_2O:EtOH mixture (50:50).[20,23] Core-shell $Au@Mo_6$ nanoparticles were synthesized by the controlled addition of a solution of $[Mo_6Br^i_8(NCS)^a_6]^{2-}$ (62μmol in EtOH) onto an aqueous solution of citrate capped AuNP (OD 0.5), and let to rest under mechanical agitation for 24h. The size of the amorphous shells was adjusted as a function of Mo_6 cluster concentration and time. A separate study which focuses on

the details of the synthesis and full characterization of these core-shell $Au@Mo_6$ nanoparticles is currently being prepared for publication. The synthesis of empty shells was performed according to a previously reported method.[20]

Imaging and electron energy-loss spectroscopy (EELS) were performed using a FEI Titan transmission electron microscope equipped with a Gatan GIF Quantum spectrometer.[43] A few drops of the water-based solutions containing the nanoparticles were deposited onto TEM grids covered by a ~6 nm C film (Ohken Shoji, SHR-C075) and allowed to dry in air. The grids were annealed for 5 min at 150 ˚C under high vacuum (~5×10^{-4} Pa) before inserting into the microscope. The TEM was operated at 80 and 300 kV in scanning (STEM) mode, with a probe current of 30 pA and an energy resolution of 150 meV set using the gun monochromator. The images were obtained using a high-angle annular dark-field (HAADF) detector. The EELS spectra and images were acquired at the same time using the spectrum imaging (SI) mode, with a pixel time of 1 ms for the low-loss (plasmon) region. The data was processed using Gatan GMS and ImageJ[44] with the Cornell Spectrum Imager add-on.[45] The low-loss EELS datasets were normalized to the total number of counts and aligned using the zero-loss peak (ZLP). The background given by the ZLP tail was fitted using a power-law function and subtracted. The

amplitude and position of the plasmon peak at each point were obtained by fitting it with a Gaussian function.

Additional imaging was performed using a JEOL SM-67F scanning electron microscope, operated at 10 kV. Optical absorption measurements were performed using a JASCO V-570 UV/Vis/NIR spectrometer, at room temperature.

The numerical values of the absorption, extinction and EELS spectra were extracted through boundary element methods using the open-source code MNPBEM.[46,47] The optical response of Au was taken from experimentally measured values of its dielectric permittivity.[48] The optical response of the cluster material was considered constant in the visible part of the electromagnetic spectrum, characterized by a dielectric constant of ε=5.5. This value was determined based on the high optical activity of Mo-containing compounds,[49] and confirmed by comparing the calculation results to the experimental data.

ASSOCIATED CONTENT

Supporting Information.

The following files are available free of charge.

HAADF images of core-shell particles with different shell thickness, MLLS fitting of EELS spectra, nanoparticle core size histogram and plasmon peak dependency, radially averaged HAADF and EELS signal profiles, SEM images and size distributions, optical absorption spectra and corresponding simulations. (PDF)

AUTHOR INFORMATION

Notes

The authors declare no competing financial interests.

ACKNOWLEDGMENT

O. C. and K. K. acknowledge funding from the Japan Society for the Promotion of Science (JSPS) through KAKENHI grant no. 20H02624. F. S. thanks the JSPS for a postdoctoral Fellowship, as well as related financial support (grant no. JP18F18797). V. K. was partially supported by JSPS KAKENHI Grant number 21K13868. Drs. T. Nagao (NIMS) and J. Henzie (NIMS) are acknowledged for fruitful discussions.

REFERENCES

(1) Barber, D. J.; Freestone, I. C. An Investigation of the Origin of the Colour of the Lycurgus Cup by Analytical Transmission Electron Microscopy. *Archaeometry* **1990**, *32*, 33–45.

(2) Mie, G. Beiträge Zur Optik Trüber Medien, Speziell Kolloidaler Metallösungen. *Annalen der Physik* **1908**, *330*, 377–445.

(3) Amendola, V.; Pilot, R.; Frasconi, M.; Maragò, O. M.; Iatì, M. A. Surface Plasmon Resonance in Gold Nanoparticles: A Review. *Journal of Physics: Condensed Matter* **2017**, *29*, 203002.

(4) Myroshnychenko, V.; Rodríguez-Fernández, J.; Pastoriza-Santos, I.; Funston, A. M.; Novo, C.; Mulvaney, P.; Liz-Marzán, L. M.; García de Abajo, F. J. Modelling the Optical Response of Gold Nanoparticles. *Chemical Society Reviews* **2008**, *37*, 1792.

(5) Maier, S. A. Plasmonics: Fundamentals and Applications. Springer, New York, **2007**.

(6) Losquin, A.; Zagonel, L. F.; Myroshnychenko, V.; Rodríguez-González, B.; Tencé, M.; Scarabelli, L.; Förstner, J.; Liz-Marzán, L. M.; García de Abajo, F. J.; Stéphan, O.; et al. Unveiling Nanometer Scale Extinction and Scattering Phenomena through Combined

Electron Energy Loss Spectroscopy and Cathodoluminescence Measurements. *Nano Letters* **2015**, *15*, 1229–1237.

(7) García de Abajo, F. J. Optical Excitations in Electron Microscopy. *Reviews of Modern Physics* **2010**, *82*, 209–275.

(8) Watanabe, H. Experimental Evidence for the Collective Nature of the Characteristic Energy Loss of Electrons in Solids–Studies on the Dispersion Relation of Plasma Frequency–. *Journal of the Physical Society of Japan* **1956**, *11*, 112–119.

(9) Mayoral, A.; Magen, C.; Jose-Yacaman, M. Nanoscale Mapping of Plasmon Resonances of Functional Multibranched Gold Nanoparticles. *Chemical Communications* **2012**, *48*, 8667.

(10) Goris, B.; Guzzinati, G.; Fernández-López, C.; Pérez-Juste, J.; Liz-Marzán, L. M.; Trügler, A.; Hohenester, U.; Verbeeck, J.; Bals, S.; Van Tendeloo, G. Plasmon Mapping in Au@Ag Nanocube Assemblies. *The Journal of Physical Chemistry C* **2014**, *118*, 15356–15362.

(11) Beauvais, L. G.; Shores, M. P.; Long, J. R. Cyano-Bridged Re_6Q_8 (Q = S, SE) Cluster-Cobalt(II) Framework Materials: Versatile Solid Chemical Sensors. *Journal of the American Chemical Society* **2000**, *122*, 2763–2772.

(12) Hernández Sánchez, R.; Zheng, S.-L.; Betley, T. A. Ligand Field Strength Mediates Electron Delocalization in Octahedral $[(^{H}L)_2Fe_6(L')_m]^{n+}$ Clusters. *Journal of the American Chemical Society* **2015**, *137*, 11126–11143.

(13) Lei, Z.; Pei, X.-L.; Guan, Z.-J.; Wang, Q.-M. Full Protection of Intensely Luminescent Gold(I)-Silver(I) Cluster by Phosphine Ligands and Inorganic Anions. *Angewandte Chemie International Edition* **2017**, *56*, 7117–7120.

(14) Wilmet, M.; Lebastard, C.; Sciortino, F.; Comby-Zerbino, C.; MacAleese, L.; Chirot, F.; Dugourd, P.; Grasset, F.; Matsushita, Y.; Uchikoshi, T.; et al. Revisiting Properties of Edge-Bridged Bromide Tantalum Clusters in the Solid-State, in Solution and Vice Versa: An Intertwined Experimental and Modelling Approach. *Dalton Transactions* **2021**, *50*, 8002–8016.

(15) Kirakci, K.; Cordier, S.; Perrin, C. Synthesis and Characterization of $Cs_2Mo_6X_{14}$ (X = Br or I) Hexamolybdenum Cluster Halides: Efficient Mo_6 Cluster Precursors for Solution Chemistry Syntheses. *Zeitschrift fur anorganische und allgemeine Chemie* **2005**, *631*, 411–416.

(16) Dierre, B.; Costuas, K.; Dumait, N.; Paofai, S.; Amela-Cortes, M.; Molard, Y.; Grasset, F.; Cho, Y.; Takahashi, K.; Ohashi, N.; et al. Mo_6 Cluster-Based Compounds for Energy Conversion Applications: Comparative Study of Photoluminescence and Cathodoluminescence. *Science and Technology of Advanced Materials* **2017**, *18*, 458–466.

(17) Cordier, S.; Grasset, F.; Molard, Y.; Amela-Cortes, M.; Boukherroub, R.; Ravaine, S.; Mortier, M.; Ohashi, N.; Saito, N.; Haneda, H. Inorganic Molybdenum Octahedral Nanosized Cluster Units, Versatile Functional Building Block for Nanoarchitectonics. *Journal of Inorganic and Organometallic Polymers and Materials* **2014**, *25*, 189–204.

(18) Amela-Cortes, M.; Cordier, S.; Naumov, N. G.; Mériadec, C.; Artzner, F.; Molard, Y. Hexacyano Octahedral Metallic Clusters as Versatile Building Blocks in the Design of Extended Polymeric Framework and Clustomesogens. *J. Mater. Chem. C* **2014**, *2*, 9813–9823.

(19) Molard, Y. Clustomesogens: Liquid Crystalline Hybrid Nanomaterials Containing Functional Metal Nanoclusters. *Accounts of Chemical Research* **2016**, *49*, 1514–1523.

(20) Sciortino, F.; Cuny, J.; Grasset, F.; Lagrost, C.; Lemoine, P.; Moréac, A.; Molard, Y.; Takei, T.; Cordier, S.; Chevance, S.; et al. The Ouzo Effect to Selectively Assemble Molybdenum Clusters into Nanomarbles or Nanocapsules with Increased HER Activity. *Chemical Communications* **2018**, *54*, 13387–13390.

(21) Grasset, F.; Dorson, F.; Cordier, S.; Molard, Y.; Perrin, C.; Marie, A.-M.; Sasaki, T.; Haneda, H.; Bando, Y.; Mortier, M. Water-in-Oil Microemulsion Preparation and Characterization of $Cs_2[Mo_6X_{14}]@SiO_2$ Phosphor Nanoparticles Based on Transition Metal Clusters (X = Cl, Br, and I). *Advanced Materials* **2008**, *20*, 143–148.

(22) Grasset, F.; Molard, Y.; Cordier, S.; Dorson, F.; Mortier, M.; Perrin, C.; Guilloux-Viry, M.; Sasaki, T.; Haneda, H. When "Metal Atom Clusters" Meet ZnO Nanocrystals: A $((n\text{-}C_4H_9)_4N)_2Mo_6Br_{14}$@ZnO Hybrid. *Advanced Materials* **2008**, *20*, 1710–1715.

(23) Kepenekian, M.; Molard, Y.; Costuas, K.; Lemoine, P.; Gautier, R.; Ababou Girard, S.; Fabre, B.; Turban, P.; Cordier, S. Red-NIR Luminescence of Mo_6 Monolayered Assembly Directly Anchored on Au(001). *Materials Horizons* **2019**, *6*, 1828–1833.

(24) Ringe, E.; Langille, M. R.; Sohn, K.; Zhang, J.; Huang, J.; Mirkin, C. A.; Van Duyne, R. P.; Marks, L. D. Plasmon Length: A Universal Parameter to Describe Size Effects in Gold Nanoparticles. *The Journal of Physical Chemistry Letters* **2012**, *3*, 1479–1483.

(25) Hartland, G. V. Optical Studies of Dynamics in Noble Metal Nanostructures. *Chemical Reviews* **2011**, *111*, 3858–3887.

(26) Novikova, E. D.; Vorotnikov, Y. A.; Nikolaev, N. A.; Tsygankova, A. R.; Shestopalov, M. A.; Efremova, O. A. The Role of Gold Nanoparticles' Aspect Ratio in

Plasmon-Enhanced Luminescence and the Singlet Oxygen Generation Rate of Mo_6 Clusters. *Chemical Communications* **2021**, *57*, 7770–7773.

(27) Campos, A.; Troc, N.; Cottancin, E.; Pellarin, M.; Weissker, H.-C.; Lermé, J.; Kociak, M.; Hillenkamp, M. Plasmonic Quantum Size Effects in Silver Nanoparticles Are Dominated by Interfaces and Local Environments. *Nature Physics* **2018**, *15*, 275–280.

(28) Mertens, H.; Koenderink, A. F.; Polman, A. Plasmon-Enhanced Luminescence near Noble-Metal Nanospheres: Comparison of Exact Theory and an Improved Gersten and Nitzan Model. *Physical Review B* **2007**, *76*, 115123.

(29) Zhu, J.; Zhang, F.; Chen, B.-B.; Li, J.-J.; Zhao, J.-W. Tuning the Shell Thickness-Dependent Plasmonic Absorption of Ag Coated Au Nanocubes: The Effect of Synthesis Temperature. *Materials Science and Engineering: B* **2015**, *199*, 113–120.

(30) Wu, W.; Njoki, P. N.; Han, H.; Zhao, H.; Schiff, E. A.; Lutz, P. S.; Solomon, L.; Matthews, S.; Maye, M. M. Processing Core/Alloy/Shell Nanoparticles: Tunable Optical

Properties and Evidence for Self-Limiting Alloy Growth. *The Journal of Physical Chemistry C* **2011**, *115*, 9933–9942.

(31) Yang, Y.-C.; Wang, H.-J.; Whang, J.; Huang, J.-S.; Lyu, L.-M.; Lin, P.-H.; Gwo, S.; Huang, M. H. Facet-Dependent Optical Properties of Polyhedral Au–Cu_2O Core–Shell Nanocrystals. *Nanoscale* **2014**, *6*, 4316.

(32) Haiying, Y.; Jian, Z.; Jianjun, L.; Junwu, Z. Shell Thickness Dependent Non-Monotonic Plasmon Shift of Gold-Protein Core–Shell Nanoparticle Thin Films. *Journal of Computational and Theoretical Nanoscience* **2011**, *8*, 1643–1647.

(33) Zhang, S.; Xu, X.; Zhang, G.; Liu, B.; Yang, J. One-Pot One-Step Synthesis of Au@SiO_2 Core–shell Nanoparticles and Their Shell-Thickness-Dependent Fluorescent Properties. *RSC Advances* **2019**, *9*, 17674–17678.

(34) Shan, J.; Chen, J.; Nuopponen, M.; Viitala, T.; Jiang, H.; Peltonen, J.; Kauppinen, E.; Tenhu, H. Optical Properties of Thermally Responsive Amphiphilic Gold Nanoparticles Protected with Polymers. *Langmuir* **2005**, *22*, 794–801.

(35) Hettler, S.; Dries, M.; Hermann, P.; Obermair, M.; Gerthsen, D.; Malac, M. Carbon Contamination in Scanning Transmission Electron Microscopy and its Impact on Phase-Plate Applications. *Micron* **2017**, *96*, 38–47.

(36) Bosman, M.; Keast, V. J.; Watanabe, M.; Maaroof, A. I.; Cortie, M. B. Mapping Surface Plasmons at the Nanometre Scale with an Electron Beam. *Nanotechnology* **2007**, *18*, 165505.

(37) Hsu, S.-C.; Liu, S.-Y.; Wang, H.-J.; Huang, M. H. Facet-Dependent Surface Plasmon Resonance Properties of Au-Cu_2O Core-Shell Nanocubes, Octahedra, and Rhombic Dodecahedra. *Small* **2014**, *11*, 195–201.

(38) Link, S.; El-Sayed, M. A. Spectral Properties and Relaxation Dynamics of Surface Plasmon Electronic Oscillations in Gold and Silver Nanodots and Nanorods. *The Journal of Physical Chemistry B* **1999**, *103*, 8410–8426.

(39) Niesen, B.; Rand, B. P.; Van Dorpe, P.; Shen, H.; Maes, B.; Genoe, J.; Heremans, P. Excitation of Multiple Dipole Surface Plasmon Resonances in Spherical Silver Nanoparticles. *Optics Express* **2010**, *18*, 19032.

(40) Fan, X.; Zheng, W.; Singh, D. J. Light Scattering and Surface Plasmons on Small Spherical Particles. *Light: Science & Applications* **2014**, *3*, e179.

(41) Neeves, A. E.; Birnboim, M. H. Composite Structures for the Enhancement of Nonlinear-Optical Susceptibility. *Journal of the Optical Society of America B* **1989**, *6*, 787.

(42) Sihvola, A., Lindell, I.V. Transmission Line Analogy for Calculating the Effective Permittivity of Mixtures with Spherical Multilayer Scatterers. *Journal of Electromagnetic Waves and Applications* **1988**, *2*, 741-756.

(43) Kimoto, K.; Kurashima, K.; Nagai, T.; Ohwada, M.; Ishizuka, K. Assessment of Lower-Voltage TEM Performance Using 3D Fourier Transform of through-Focus Series. *Ultramicroscopy* **2012**, *121*, 31–37.

(44) Schneider, C. A.; Rasband, W. S.; Eliceiri, K. W. NIH Image to Imagej: 25 Years of Image Analysis. *Nature Methods* **2012**, *9*, 671–675.

(45) Cueva, P.; Hovden, R.; Mundy, J. A.; Xin, H. L.; Muller, D. A. Data Processing for Atomic Resolution Electron Energy Loss Spectroscopy. *Microscopy and Microanalysis* **2012**, *18*, 667–675.

(46) García de Abajo, F. J.; Howie, A. Retarded Field Calculation of Electron Energy Loss in Inhomogeneous Dielectrics. *Physical Review B* **2002**, *65*, 115418.

(47) Hohenester, U.; Trügler, A. MNPBEM – A Matlab Toolbox for the Simulation of Plasmonic Nanoparticles. *Computer Physics Communications* **2012**, *183*, 370–381.

(48) Johnson, P. B.; Christy, R. W. Optical Constants of the Noble Metals. *Physical Review B* **1972**, *6*, 4370–4379.

(49) Lajaunie, L.; Boucher, F.; Dessapt, R.; Moreau, P. Strong Anisotropic Influence of Local-Field Effects on the Dielectric Response of α-MoO_3. *Physical Review B* **2013**, *88*, 115141.